Chapter 3
Classical Cyclotron

Abstract This tutorial is an introduction to the classical cyclotron, with hints at spin dynamics, hands-on: by numerical simulation. It begins with a brief reminder of the historical context, and then introduces the theoretical material needed for the subsequent simulation exercises.

Basic charged particle optics and acceleration concepts are addressed in this chapter, including
- closed orbit in a cyclic accelerator,
- weak focusing in a dipole magnet,
- periodic transverse motion,
- revolution period and isochronism,
- voltage gap and resonant acceleration,
- the cyclotron equation.

Simulations of a cyclotron dipole just requires the optical element DIPOLE, an analytical modeling of the field. It may be chosen to use TOSCA however, if a field map of the cyclotron magnet (computed or measured) is available. The only other optical element which will be needed is CAVITE, to simulate an oscillating voltage gap. Simulations also introduce to the default output listing zgoubi.res, to optional output files such as zgoubi.plt produced by setting IL=2 in optical elements, zgoubi.CAVITE.out produced by CAVITE, zgoubi.MATRIX.out produced by MATRIX, and other similar zgoubi.*.out output files aimed at data post-treatment, including producing graphs. Additional keywords are introduced, including FIT[2], a matching procedure; FAISCEAU which allows logging local particle coordinates in zgoubi.res; FAISTORE which logs local particle coordinates in a user defined file, usually for further external data treatment or plotting; MARKER; the 'system call' command SYSTEM; REBELOTE, a 'do loop'; and some more. Spin motion will be solved as well, this will require introducing SPNTRK, a request to do so while raytracing, and SPNPRT which prints out spin vector components to zgoubi.res.

Notations used in the Text

B; B_0	field value; at reference radius R_0
$\mathbf{B}$; B_R; B_y	field vector; radial component; axial component
$B\rho = p/q$	particle rigidity
C; C_0	orbit length, $C = 2\pi R$; reference, $C_0 = 2\pi R_0$
E	particle energy
$f_{\rm rf}$; h	RF frequency; RF harmonic number
$k = \frac{R}{B}\frac{dB}{dR}$	radial field index
m; m_0; M	mass; rest mass; in units of MeV/c^2
$\mathbf{p}$; p; p_0	particle momentum vector; its modulus; reference
q	particle charge
R; R_0; R_E	orbital radius; reference radius $R(p_0)$; at energy E
s	path variable
$\mathbf{v}$; v	particle velocity vector; its modulus
V(t); $\hat{V}$	oscillating voltage; its peak value
x, x', y, y'	radial and axial coordinates in the moving frame [(*)' = d(*)/ds]

$\beta = v/c$; β_0; β_s	normalized particle velocity; reference; synchronous
$\gamma = E/m_0$	Lorentz relativistic factor
Δp, δp	momentum offset
ϵ_u	Courant-Snyder invariant (u: x, r, y, l, Y, Z, s, etc.)
ϕ	RF phase at particle arrival at the voltage gap

Introduction

The cyclotron is the first cyclic accelerator. The concept: resonant acceleration of particles circling in a uniform magnetic field, goes back to the late 1920s [1]. The

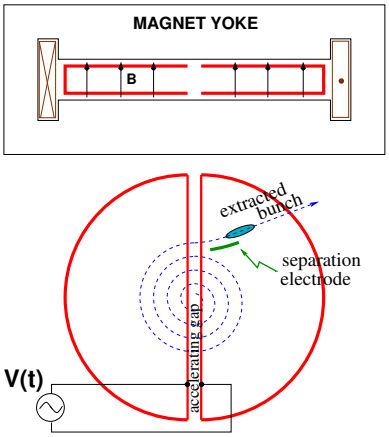

Fig. 3.1 A sketch of the classical cyclotron. In the uniform magnetic field between two circular poles (top) an ion spirals out (bottom). A double-dee (or a a single-dee facing a slotted electrode) forms a gap to which a fixed-frequency oscillating voltage V(t) is applied. Its oscillation frequency is a harmonic of the revolution frequency. Particles experiencing proper voltage phase at the gap are accelerated. A septum electrode allows bunch extraction

first cyclotron was constructed at Berkeley, acceleration of H_2^+ hydrogen ions to 80 keV [2] was achieved in 1931. The apparatus used a single dee vis-à-vis a slotted electrode forming a voltage gap, the ensemble housed in a 5 inch diameter vacuum chamber and placed in the 1.3 Tesla field of an electromagnet (Fig. 3.1). A $\approx$ 12 MHz vacuum tube oscillator a 1 kVolt peak gap voltage.

The goal foreseen in developing this technology was the acceleration of protons to MeV kinetic energy range for the study of atom nucleus - and in background a wealth of potential applications. An 11 inch cyclotron delivering a 0.01 μA H_2^+ beam at 1.22 MeV [3], and then a 27 inch cyclotron reaching 6 MeV (Fig. 3.2), followed [4]. In the wake of Cockcroft and Walton first artificial disintegration experiment, targets were mounted at the periphery of the 11 inch cyclotron, disintegrations were observed in 1932. And in 1933: *'The neutron had been identified by Chadwick in* 1932*. By* 1933 *we were producing and observing neutrons from every target bombarded by deuterons.“* [4, M.S. Livingston,p. 22].

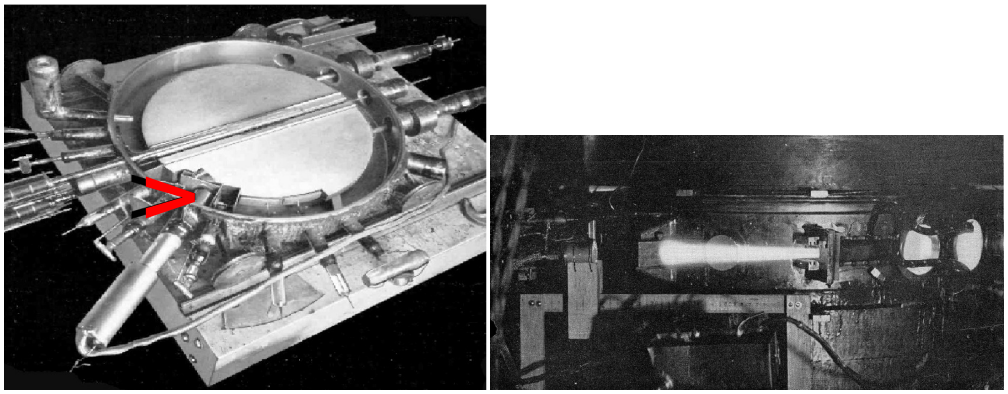

Fig. 3.2 Berkeley 27 inch cyclotron, first operated in 1934, accelerated deuterons up to 6 MeV. Left: a double-dee (seen in the vacuum chamber, cover off)), 22 inch diameter, creates an accelerating gap: 13 kV, 12 MHz radio frequency voltage is applied for deuterons for instance (through two feed lines seen on the right). This apparatus was dipped in the 1.6 Tesla dipole field of a 27 in diameter (75 ton) electromagnet. A slight decrease of the dipole field with radius, from the center of the dees, assured vertical beam focusing. Particles spiral out from the center of the dees to the rim (where they strike a target, seen at the bottom on the left - arrow). Right: ionization of the air by the extracted beam (1936); the view also shows the vacuum chamber squeezed between the pole pieces of the electromagnet

The scope with accelerated beams from cyclotrons was broad: *“At this time biological experiments were started. I can recall the first time that a mouse was irradiated with neutrons. We put the mouse in a little cage and stuck him up on the side of the cyclotron tank and left him there for a while. Of course, nothing happened because* [*etc.*]*”* [4, McMillan,p. 26]; and *“Also at about this same time the first radioactive tracer experiments on human beings were tried”* [op.cit.]; *“*[...] *simple beginnings of therapeutic use, coming a little bit later, in which neutron radiation was used, for instance, in the treatment of cancer. These things have gone on and built up*

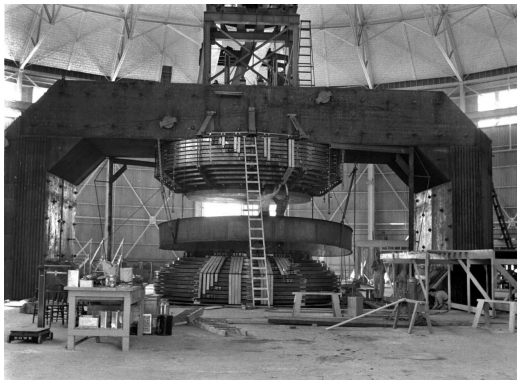

Fig. 3.3 Berkeley 184 in cyclotron. It was modified into a synchrocyclotron in 1946

so that there's now a whole field" [op.cit.]; and *"Another highlight from* 1936 *was the first time that anyone tried to make artificially a naturally occurring radionuclide."* (a bismuth isotope) [op.cit.]. The period also saw beam extraction developments (Fig. 3.2). Cyclotrons were constructed in many laboratories worldwide, from the early 1930s, following Berkeley demonstration.

Limitation in energy

An advanced theoretical understanding of the cyclotron more or less took until the mid-1930s, ending up with two news, a bad one and a good one, bad one first:

(i) the energy limitation, a consequence of the loss of isochronism resulting from the relativistic increase of the ion mass: "[...] *it seems useless to build cyclotrons of larger proportions than the existing ones* [...] *an accelerating chamber of* 37 *in radius will suffice to produce deuterons of* 11 *MeV energy which is the highest possible* [...]" [5] (related simulations will conclude this Chapter, "Classical Cyclotron"), or in a different form: "*If you went to graduate school in the* 1940*s, this inequality* $(-1 < k < 0)$ *was the end of the discussion of accelerator theory*" [6].

The good news next:

(ii) the overcoming of that relativistic limit, due to L.H. Thomas in 1938 [7] - it took a few years though, to see practical effects.

Classical cyclotron technology has been in use for some time up to the few tens of MeV/u that it allows (Fig. 3.4), for such applications as neutron production for material science, radio-isotope production for medicine, injector stages in cyclotron complex facilities [9]. However with the progress in magnet computation tools and magnet fabrication (including permanent magnet techniques [10]), and the progress in computational speed and beam dynamics simulations (which includes accurate raytracing, as concerned in the present opus), the azimuthally varying field (AVF, or Thomas' [7]) cyclotron, much more performing, comes out to be essentially as simple and has in a general manner prevailed (Fig. 3.4).

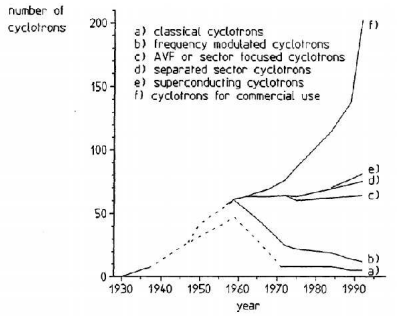

Fig. 3.4 Evolution of cyclotron species, over the years [8, Fig. 8]

3.1 Theory, Basic Concepts

The cyclotron was conceived as a means to overcome the inconvenient of using a long series of high voltage electrodes in a linear layout, by, instead, repeated recirculation using a magnetic field, for incremental, resonant, energy gain through a single accelerating gap. This gap is formed by a pair of cylindrical electrodes,

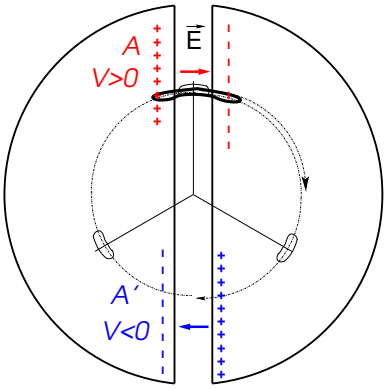

Fig. 3.5 Resonant acceleration: a positive ion bunch meets an accelerating field **E** across gap A, at time t; it meets again, half a revolution later, at time t + $T_{rev}/2$, an accelerating field across gap A', and so on so forth. In this $h = 1$ configuration, one bunch (and only one) over a turn is in synchronism with the accelerating phase of the oscillating voltage, at both gaps. Higher h allows more bunches: the next possibility with two dees would be h=3, and three stable bunches at 120 degrees from one another (thin contours) over a turn

"dees" (Fig. 3.5) which are applied a fixed frequency oscillating voltage, generated using a radio transmitter. The dees are placed in a uniform magnetic field which causes the ion bunches to follow, as they are accelerated, a piecewise-circular motion with increasing radius, normal to the field, more or less in phase with the voltage oscillation. An oscillating voltage is necessary as a DC voltage gap (a conservative field) in a circular accelerator can not yield energy gain: with the advent of resonant acceleration in the cyclotron and the development of cyclic accelerators in the horizon, it is interesting to note in passing that it is not possible to accelerate a particle

traveling on a closed path using an electrostatic field ($\mathbf{E} = -\mathbf{grad}\mathrm{V}(\mathbf{R}, \mathrm{t})$ derives from a scalar potential), as the work by $\mathbf{F} = q\mathbf{E}$ only depends on the initial and final states, it does not dependent on the path followed (Fig. 3.6), which can be written

$$W = \int_P^Q \mathbf{F}.d\mathbf{s} = -q \int_P^Q \mathbf{grad}V.d\mathbf{s} = -q(V_Q - V_P) \tag{3.1}$$

On a closed path: $\oint \mathbf{F}.d\mathbf{s} = 0$, the force is conservative, no work is performed, consequence: a DC voltage gap in a circular machine does not yield energy gain.

Instead, the work of a force of induction origin, where $\mathbf{E} = -\partial\mathbf{A}/\partial\mathrm{t}$ arises from the variation of a magnetic flux ($\mathbf{B} = \mathbf{curl}\,\mathbf{A}$, $\mathbf{A}$ a vector potential), may be non-zero on a closed path. This is achieved for instance using a radio-frequency system which feeds an oscillating voltage across a gap, $\mathrm{V(t)} = \hat{\mathrm{V}}\sin(\omega_{\mathrm{rf}}\mathrm{t} + \phi)$ (Fig. 3.7).

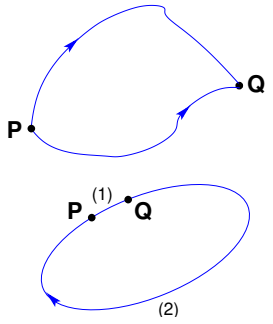

Fig. 3.6 Top: the work of the electrostatic force $\mathbf{F} = q\mathbf{E}$ is $W = \int_P^Q \mathbf{F}.d\mathbf{s} = -q(V_Q - V_P)$. Bottom: over closed path, the particle loses along (2) the energy gained along (1)

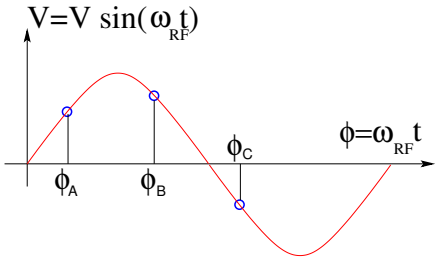

Fig. 3.7 A particle which reaches the double-dee gap at the RF phase $\omega_{\mathrm{rf}}\mathrm{t} = \phi_{\mathrm{A}}$ or $\omega_{\mathrm{rf}}t = \phi_B$ is accelerated. If it reaches the gap at $\omega_{\mathrm{rf}}\mathrm{t} = \phi_{\mathrm{C}}$ it is decelerated

As an accelerated bunch spirals outward in a uniform magnetic field, the increase in the distance it travels over a turn is compensated by its velocity increase: in the non-relativistic approximation ($\beta \ll 1$), the revolution period $\mathrm{T_{rev}}$ increases only slowly with energy; with appropriate voltage frequency $\mathrm{f_{rf}} \approx \mathrm{h/T_{rev}}$ revolution motion and RF can be maintained in sufficiently close synchronism, $\mathrm{T_{rev}} \approx \mathrm{hT_{rf}}$, that the bunch will transit the accelerating gaps (Fig. 3.5) during the accelerating phase of the oscillating V(t) (Fig. 3.7).

The orbital motion quantities: radius R, field B, particle rigidity BR, revolution frequency $f_{rev} = \omega_{rev}/2\pi$, satisfy

$$BR = \frac{p}{q}, \qquad 2\pi f_{rev} = \frac{v}{R} = \frac{qB}{m} = \frac{qB}{\gamma m_0} \tag{3.2}$$

These relationships hold at all γ, from $v \ll c$ ($\gamma \approx 1$, domain of the *classical* cyclotron) to $\gamma > 1$ (domain of the *isochronous* cyclotron). To give an idea of the revolution frequency, in the limit $\gamma = 1$ one has

$$\frac{f_{rev}}{B} = \frac{q}{2\pi m} = 15.25\,\mathrm{MHz/T} \quad \text{for protons.}$$

The RF frequency $f_{rf} = \omega_{rf}/2\pi$ is constant in a cyclotron, whereas the revolution period slowly increases with energy (Sec. 3.1.3). In the classical cyclotron f_{rf} is set, by design, equal to hf_{rev} for an intermediate energy taken along the acceleration cycle. The energy gain, or loss, by the particle when transiting the gap is

$$\Delta W = q\hat{V}\sin\phi(t) \quad \text{with } \phi(t) = \omega_{rf}t - \omega_{rev}t + \phi_0 \tag{3.3}$$

with ϕ its phase with respect to the RF signal at the gap (*e.g.*, ϕ_A, ϕ_B or ϕ_C in Fig. 3.7) and ϕ_0 the value at $t = 0$, $\omega_{rev}t$ the orbital angle advance.

Fixed-frequency acceleration requires the RF and cyclotron frequencies to be matched to one another. However the relativistic increase of the mass upon velocity increase causes the revolution period to increase with momentum: in $T_{rev} = 2\pi m/qB$, B is almost constant and m increases, resulting in a turn-by-turn

$$\frac{\Delta T_{rev}}{T_{rev}} = \gamma - 1$$

The mis-match between the accelerating RF and cyclotron frequencies is a turn-by-turn cumulative effect and sets a limit to the tolerable isochronism defect, $\Delta T_{rev}/T_{rev} \approx 2-3\%$, or highest velocity $\beta = v/c \approx 0.22$. This results for instance in a practical limitation of the "classical cyclotron" to an upper ≈ 25 MeV for protons, and ≈ 50 MeV for D and α particles.

To conclude on these basis concepts regarding acceleration, multiple accelerating gap structures is part of the evolutions of the classical cyclotron, where a "D" is rather a "Δ" pattern, and towards high RF frequency harmonic. An example among many others is, as an illustration, GANIL C0 injector with its 4 accelerating gaps and h=4 and h=8 RF operation [9].

3.1.1 Fixed-Energy Orbits, Revolution Period

The differential equations of particle motion are established in the Serret-Frénet frame, Sec. 3.1.2, however, some basic geometrical properties can be derived in the

laboratory frame, as follows. In the laboratory frame (O;x,y,z), with (O;x,z) the bend plane, assume $\mathbf{B}|_{y=0} = \mathbf{B}_y$. A particle is launched from the origin with a velocity $\mathbf{v} = (v \sin\alpha, 0, v \cos\alpha)$ at an angle α from the longitudinal axis z (Fig. 3.8).

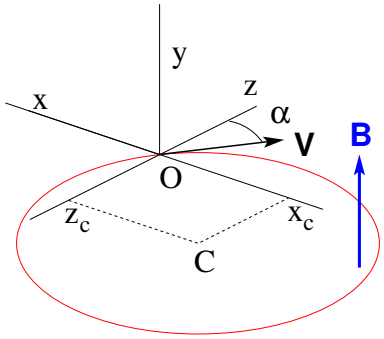

Fig. 3.8 Circular motion of a charged particle in the plane normal to a uniform magnetic field **B**. The circle center is at $x_C = -v\cos\alpha/\omega_{\text{rev}}$, $z_C = v\sin\alpha/\omega_{\text{rev}}$,

Solving

$$m\dot{\mathbf{v}} = q\mathbf{v}\times\mathbf{B} \tag{3.4}$$

with $\mathbf{v} = (\dot{x}, \dot{y}, \dot{z})$, $\mathbf{B} = (0, B_y, 0)$ yields the parametric equations of motion

$$\begin{cases} x(t) = \dfrac{v}{\omega_{\text{rev}}}\cos(\omega_{\text{rev}}t - \alpha) - \dfrac{v\cos\alpha}{\omega_{\text{rev}}} \\ z(t) = \dfrac{v}{\omega_{\text{rev}}}\sin(\omega_{\text{rev}}t - \alpha) + \dfrac{v\sin\alpha}{\omega_{\text{rev}}} \\ y(t) = \text{constant} \end{cases} \tag{3.5}$$

which results in

$$\left(x + \frac{v\cos\alpha}{\omega_{\text{rev}}}\right)^2 + \left(z - \frac{v\sin\alpha}{\omega_{\text{rev}}}\right)^2 = \left(\frac{v}{\omega_{\text{rev}}}\right)^2 \tag{3.6}$$

a circular trajectory of radius $R = p/qB$ centered at $x = -v\cos\alpha/\omega_{\text{rev}}$, $z = v\sin\alpha/\omega_{\text{rev}}$, revolution period

$$T_{rev} = \frac{2\pi}{\omega_{rev}} = \frac{2\pi m}{qB}$$

Cyclic motion - Horizontal motion in uniform field has no privileged reference orbit: for a given momentum, the initial radius and velocity vector define a particular closed, circular orbit. A particle launched with an axial velocity component v_y on the other hand, drifts vertically linearly with time, as there is no axial restoring force. The next

Section will investigate the necessary field property, absent in our simplified field model so far, proper to ensure confinement of the multiturn 6-dimensional periodic motion in the vicinity of the median plane of the cyclotron dipole magnet.

3.1.2 Weak Focusing, Transverse Motion

In the lower energy (smaller radius) accelerated turns in a classical cyclotron, the electric field in the accelerating gap contributes proper transverse focusing so that the magnet gap can be designed parallel (an example can be found in Ref. [9]). In very low energy applications even, extraction energy in the tens of keV/u range where electric fields are still effective, flat magnetic field with uniformity $dB/B < 10^{-4}$ can be achieved over the (reduced) extent of the cyclotron orbit and maintains proper isochronism. Beyond this low energy region however, at greater radius, a magnetic field gradient must be introduced, field decreasing with R, by shaping the magnet poles, to ensure proper vertical focusing. Note that because of the field decreases with R in a parallel gap, as discovered *a posteriori*, the very first cyclotrons were working [11]. This section introduces to these magnetic focusing principles.

In the following, $B_R(R)$, $B_y(R)$ denote the radial and axial components of the magnetic field at radius R. Median-plane symmetry of the field is assumed, thus $B_R|_{y=0} = 0$ at all R (Fig. 3.9). Particle coordinates are defined in the Serret-Frénet frame (O;s,x,y), moving along the R_0 radius reference orbit (the origin O is at the location of the reference particle, s axis tangent to the reference orbit, x axis radial, y axis normal to the bend plane, Fig. 3.10). The radial excursion of a particle with respect to the reference orbit writes

$$x(t) = R(t) - R_0 \ll R_0 \tag{3.7}$$

Considering small radial and axial excursions from ($R = R_0, y = 0$), a Taylor expansion of the magnetic field can be introduced,

$$\begin{aligned} B_y(R_0 + x) &= B_y(R_0) + x \left.\frac{\partial B_y}{\partial R}\right|_{R_0} + \frac{x^2}{2!} \left.\frac{\partial^2 B_y}{\partial R^2}\right|_{R_0} + \ldots \approx B_y(R_0) + x \left.\frac{\partial B_y}{\partial R}\right|_{R_0} \\ B_R(0 + y) &= y \underbrace{\left.\frac{\partial B_R}{\partial y}\right|_0}_{= \left.\frac{\partial B_y}{\partial R}\right|_{R_0}} + \frac{y^3}{3!} \left.\frac{\partial^3 B_R}{\partial y^3}\right|_0 + \ldots \approx y \left.\frac{\partial B_y}{\partial R}\right|_{R_0} \end{aligned} \tag{3.8}$$

Using this approximation, the differential equations of motion in the moving frame can be written under the form, linear in x and y,

$$F_x = m\ddot{x} = -qvB_y(R) + \frac{mv^2}{R_0 + x} \approx -qv\left(B_y(R_0) + \left.\frac{\partial B_y}{\partial R}\right|_{R_0} x\right) + \frac{mv^2}{R_0}\left(1 - \frac{x}{R_0}\right)$$

$$\rightarrow m\ddot{x} = -\frac{mv^2}{R_0^2}\left(\frac{R_0}{B_0}\left.\frac{\partial B_y}{\partial R}\right|_{R_0} + 1\right)x \tag{3.9}$$

$$F_y = m\ddot{y} = qvB_R(y) = qv\left.\frac{\partial B_R}{\partial y}\right|_{y=0} y + \text{higher order} \rightarrow m\ddot{y} = qv\frac{\partial B_y}{\partial R}y$$

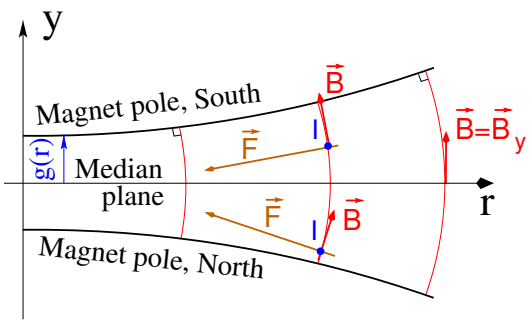

Fig. 3.9 Axial motion stability requires proper shaping of field lines: B has to decrease with radius. The Laplace force pulls a charge at I (velocity pointing out of the page) toward the median plane. Increasing the field gradient (k closer to -1, gap opening up faster) increases the focusing

982

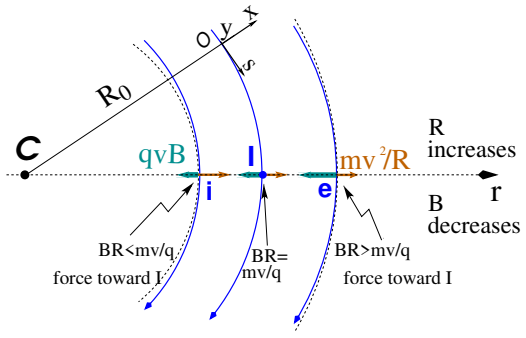

Fig. 3.10 Radial motion stability in an axially symmetric structure. Arrowed arcs are trajectories of particles with momentum p=mv. Dashed arcs are centered at C, center of the cyclotron. The resultant $F_t = -qvB + mv^2/r$, is zero at I: $B_0R_0 = mv/q$. The resultant at i is toward I if $qvB_i < mv^2/R_i$, *i.e.* $B_iR_i < mv/q$; the resultant at e is toward I if $qvB_e > mv^2/R_e$, *i.e.* $B_eR_e > mv/q$

983 Note $B_y(R_0) = B_0$ and introduce

$$\omega_R^2 = \omega_{rev}^2\left(1 + \frac{R_0}{B_0}\frac{\partial B_y}{\partial R}\right), \quad \omega_y^2 = -\omega_{rev}^2\frac{R_0}{B_0}\frac{\partial B_y}{\partial R} \tag{3.10}$$

984 equations 3.9 can thus be written under the form

$$\ddot{x} + \omega_R^2 x = 0 \qquad \text{and} \qquad \ddot{y} + \omega_y^2 y = 0 \tag{3.11}$$

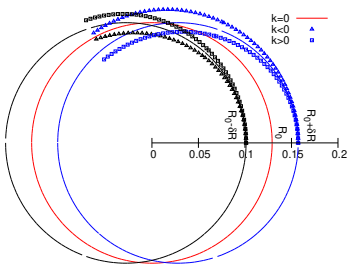

Fig. 3.11 Geometrical focusing: in a flat field, k=0, the two circular trajectories at $r = R_0 \pm \delta R$ (solid lines) undergo exactly one oscillation around the reference orbit $r = R_0$. A positive k increases the convergence (square markers - but then the vertical motion diverges from the median plane), a negative k decreases the convergence (triangles)

A restoring force (linear terms in x and y, Eq. 3.11) arises from the radially varying field, characterized by a field index

$$\mathrm{k} = \frac{\mathrm{R}_0}{\mathrm{B}_0}\frac{\partial \mathrm{B}_\mathrm{y}}{\partial \mathrm{R}}\bigg|_{\mathrm{R}=\mathrm{R}_0,\mathrm{y}=0} \tag{3.12}$$

and adds in the radial motion to the focusing due to the curvature (the term "1" in ω_R^2, Eq. 3.10).

Axial stability in a cyclotron requires a restoring force directed toward the median plane. Referring to Fig. 3.9, this means $\mathrm{F_y} = -\mathrm{ay}$ (with the a factor some positive quantity) and thus $\mathrm{B_R} < 0$, at all (r, $y \neq 0$). This is achieved by designing a guiding field which decreases with radius, $\frac{\partial B_R}{\partial y} < 0$. Referring to Eq. 3.12 this translates into $\mathrm{k} < 0$.

Radial stability in a constant field is a geometrical property, resulting from the curvature of the trajectory (Fig. 3.11). In a weakly decreasing field B(R) on the other hand, a particle with momentum p = mv sinusoiding around the R_0-radius reference circle experiences in the Serret-Frénet frame a total force $F_t = -qvB + m\frac{v^2}{r}$ (Fig. 3.10) of which the (outward) component $\mathrm{f_c} = \mathrm{m}\frac{\mathrm{v}^2}{\mathrm{r}}$ decreases with r at a higher rate than the decrease of the Laplace (inward) component $\mathrm{f_B} = -\mathrm{qvB(r)}$. In other words, radial stability requires BR to increase with R, $\frac{\partial \mathrm{BR}}{\partial \mathrm{R}} = \mathrm{B} + \mathrm{R}\frac{\partial \mathrm{B}}{\partial \mathrm{R}} \geq 0$, this holds in particular at $\mathrm{R_0}$, thus $1 + \mathrm{k} \geq 0$.

The condition for transverse motion stability around the circular equilibrium orbit results from these axial and radial stability conditions, namely,

$$-1 \leq \mathrm{k} < 0 \tag{3.13}$$

Note regarding the geometrical focusing: the focal distance associated with the curvature of a magnet of arc length $\mathcal{L}$ is obtained by integrating $\frac{\mathrm{d}^2\mathrm{x}}{\mathrm{ds}^2} + \frac{1}{\mathrm{R}_0^2}\mathrm{x} = 0$ and identifying with the focusing property $\Delta \mathrm{x}' = -\mathrm{x}/\mathrm{f}$, namely,

$$\Delta x' = \int \frac{d^2x}{ds^2} ds \approx \frac{-x}{R^2} \int ds = \frac{-x\mathcal{L}}{R^2}, \quad \text{thus} \quad f = \frac{R^2}{\mathcal{L}}$$

Isochronism

The relativistic increase of the mass precludes strict isochronism: the revolution frequency slowly decreases with the energy of the particle on its spiraling out trajectory (Eq. 3.2). The focusing condition $-1 < k < 0$ (B deceasing with R) further contributes breaking the isochronism by virtue of $\omega_{rev} \propto B$. As a consequence, the phase of the oscillating voltage at arrival of a particle at the accelerating gap (the so-called RF phase) changes turn after turn. This is addressed further in Sec. 3.1.3.

Paraxial Transverse Coordinates

Introducing the path variable, s, as the independent variable in Eq. 3.11 and using the approximation $ds \approx v dt$ (*i.e.*, neglecting the transverse velocity components), the equations of motion in the moving frame (Eq. 3.11) take the form

$$\frac{d^2x}{ds^2} + \frac{1+k}{R_0^2} x = 0 \qquad \text{and} \qquad \frac{d^2y}{ds^2} - \frac{k}{R_0^2} y = 0 \tag{3.14}$$

Given $-1 < k < 0$ the motion is that of a harmonic oscillator, in both planes, with respective restoring constants $(1+k)/R_0^2$ and $-k/R_0^2$, both positive quantities. The solution is a sinusoidal motion,

$$\begin{cases} R(s) - R_0 = x(s) = x_0 \cos \frac{\sqrt{1+k}}{R_0}(s - s_0) + x_0' \frac{R_0}{\sqrt{1+k}} \sin \frac{\sqrt{1+k}}{R_0}(s - s_0) \\ R'(s) = x'(s) = -x_0 \frac{\sqrt{1+k}}{R_0} \sin \frac{\sqrt{1+k}}{R_0}(s - s_0) + x_0' \cos \frac{\sqrt{1+k}}{R_0}(s - s_0) \end{cases} \tag{3.15}$$

$$\begin{cases} y(s) = y_0 \cos \frac{\sqrt{-k}}{R_0}(s - s_0) + y_0' \frac{R_0}{\sqrt{-k}} \sin \frac{\sqrt{-k}}{R_0}(s - s_0) \\ y'(s) = -y_0 \frac{\sqrt{-k}}{R_0} \sin \frac{\sqrt{-k}}{R_0}(s - s_0) + y_0' \cos \frac{\sqrt{-k}}{R_0}(s - s_0) \end{cases} \tag{3.16}$$

The dissymmetry between the two frequencies, a "1" in "$\sqrt{1+k}$" compared to $\sqrt{-k}$, stems from the geometrical focusing resulting from the curvature.

Two wave numbers may be introduced,

$$\nu_R = \frac{\omega_R}{\omega_{rev}} = \sqrt{1+k} \quad \text{and} \quad \nu_y = \frac{\omega_y}{\omega_{rev}} = \sqrt{-k} \tag{3.17}$$

i.e., the number of sinusoidal oscillations of the paraxial motion about the reference circular orbit over a turn, respectively radial and axial. Both are less than 1: there is less than one sinusoidal oscillation in a revolution. In addition, as a result of the revolution symmetry,

$$\nu_R^2 + \nu_y^2 = 1 \tag{3.18}$$

Phase Space

Phase space at an azimuth s around the ring is a Cartesian space with, regarding transverse particle motion, position as the horizontal axis and angle as the vertical axis, *i.e.*, $(x(s),\ x'(s) = dx/ds)$ and $(y(s),\ y'(s) = dy/ds)$ (Eqs. 3.15 3.16), or akin quantities, this is illustrated in Fig. 3.12.

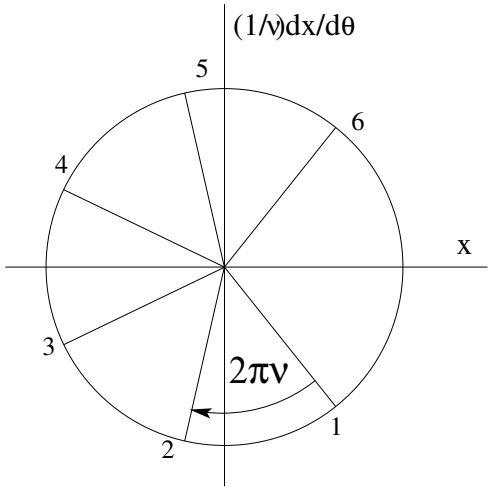

Fig. 3.12 Particle motion observed in transverse horizontal phase space at some fixed azimuth $s = R\theta_{\text{obs}}$ along the cyclotron circumference, at successive times (or turns: 1, 2, 3, ...). The horizontal axis here is $x(\theta_{\text{obs}})$, the vertical axis is $\frac{1}{\nu_R}\frac{dx}{d\theta}\Big|_{\theta=\theta_{\text{obs}}}$, using these coordinates the motion is on a circle of radius $\hat{x}$. Note that $\{x(\theta_{\text{obs}}) = \hat{x}\cos(\nu_R\theta_{\text{obs}} + \phi)$ and $\frac{1}{\nu_R}\frac{dx}{d\theta}\Big|_{\theta=\theta_{\text{obs}}} = -\hat{x}\sin(\nu_R\theta_{\text{obs}} + \phi)\}$ establishes that phase space motion is clockwise

Longitudinal phase space coordinates are the RF phase ϕ (Fig. 3.7, Eq. 3.3) and energy offset, or akin quantities.

A point in phase space represents the position of a particle at azimuth s at time t.

Particle motion over time depends on the field experienced and on two initial conditions (initial position and angle, or RF phase and energy offset, ...). It is impossible for two trajectories with different origins to coincide in phase space, at any azimuth.

Off-Momentum Motion

Momenta of particles that make up a bunch accelerated in a cyclotron span some extent $\pm\Delta p/p$.

In an axially symmetric structure, the equilibrium trajectory at momentum $\begin{cases} p_A \\ p_B = p_A + \Delta p \end{cases}$ is at radius $\begin{cases} R_A \text{ such that } B_A R_A = p_A/q \\ R_B \text{ such that } B_B R_B = p_B/q \end{cases}$, with $\begin{cases} B_B = B_A + \left(\frac{\partial B}{\partial x}\right)_0 + \ldots \\ R_B = R_A + \Delta x \end{cases}$

On the other hand

$$B_B R_B = \frac{p_B}{q} \Rightarrow \left[B_A + \left(\frac{\partial B}{\partial x}\right)_0 \Delta x + \ldots\right](R_A + \Delta x) = \frac{p_A + \Delta p}{q} = \frac{p_A}{q} + \frac{\Delta p}{q}$$

thus, neglecting terms in $(\Delta x)^2$,

$$B_A R_A + \left(\frac{\partial B}{\partial x}\right)_0 R_A \Delta x + B_A \Delta x = \frac{p_A}{q} + \frac{\Delta p}{q},$$

which, given $B_A R_A = \frac{p_A}{q}$, leaves $\Delta x \left[\left(\frac{\partial B}{\partial x}\right)_A R_A + B_A\right] = \frac{\Delta p}{q}$, which given $k = \frac{R_A}{B_A}\left(\frac{\partial B}{\partial x}\right)_0$ yields

$$\Delta x = \frac{R_A}{1+k}\frac{\Delta p}{p_A} \tag{3.19}$$

Drop the indices, take p as a reference momentum and R as the corresponding

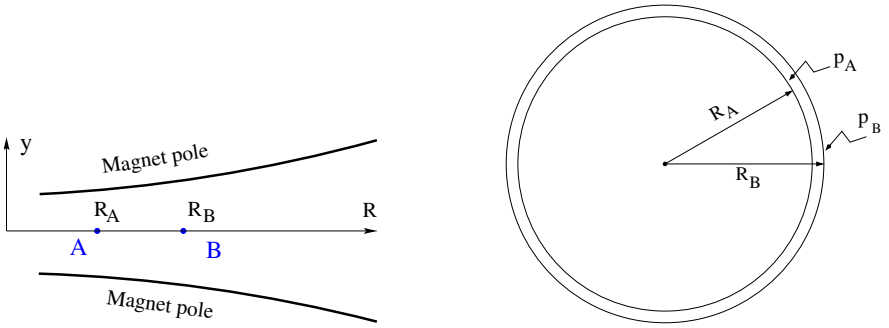

Fig. 3.13 The equilibrium radius at location A is $R = R_A$, the equilibrium momentum is p_A, rigidity $BR = B_A R_A$. The equilibrium radius at B is $R = R_B$, equilibrium momentum p_B, rigidity $BR = B_B R_B$

reference orbit radius, this leaves

$$\Delta x = D\frac{\Delta p}{p} \qquad \text{with} \qquad D = \frac{R}{1+k}, \quad \text{dispersion function} \tag{3.20}$$

The dispersion D is an s-independent quantity in the classical cyclotron as a result of the cylindrical symmetry of the field (k and R=p/qB are s-independent), and varies with R and k(R).

To the first order in the coordinates, the vertical coordinates y(s), y'(s) (Eq. 3.16) are unchanged under the effect of a momentum offset, the horizontal trajectory angle x'(s) is unchanged as well (the circular orbits are concentric, Fig. 3.13) whereas

$$x(s, p + \Delta p) = x(s, p) + \Delta p \left.\frac{dx}{dp}\right|_{s,p} = x(s) + D\frac{\Delta p}{p} \tag{3.21}$$

with $x(s)$ as in Eq. 3.15.

Orbit and revolution period lengthening

Momentum offset results in closed orbit lengthening $\delta C/C = \delta R/R \equiv \delta x/R$, which, given Eq. 3.20, can be written under the form

$$\frac{\delta C}{C} = \alpha \frac{\delta p}{p} \quad \text{with} \quad \alpha = \frac{1}{1+k} = \frac{1}{\nu_R^2} \tag{3.22}$$

with α the "momentum compaction" and $\alpha > 0$, the closed orbit length increases with momentum.

The change in revolution period $T_{\mathrm{rev}} = C/\beta c$ with momentum writes

$$\frac{\delta T_{\mathrm{rev}}}{T_{\mathrm{rev}}} = \frac{\delta C}{C} - \frac{\delta \beta}{\beta} = (\alpha - \frac{1}{\gamma^2})\frac{\delta p}{p} \tag{3.23}$$

Given that $-1 < k < 0$ and $\gamma \gtrsim 1$, it results that $\alpha - 1/\gamma^2 > 0$ thus $\delta T_{\mathrm{rev}}/T_{\mathrm{rev}} > 0$ as expected: the revolution period increases with energy, the increase in radius is faster than the velocity increase.

3.1.3 Quasi-Isochronous Resonant Acceleration

An oscillating radio-frequency (RF) electric field, with fixed-frequency $\mathrm{f_{rf}}$ is applied across the gap between the two dees (Fig. 3.1). An ion of charge q reaching the gap at time t undergoes a change in energy

$$\Delta \mathrm{W(t)} = \mathrm{q}\hat{\mathrm{V}} \sin\phi\,, \qquad \text{with} \quad \phi = \omega_{\mathrm{rf}}\mathrm{t} - (\omega_{\mathrm{rev}}\mathrm{t} + \phi_0) \tag{3.24}$$

with ϕ the RF phase experienced by the particle at the time it crosses the gap and ϕ_0 the origin in phase for the particle motion. This ignores the "transit time", the effect of the time that the particle spends across the gap on the overall energy gain.

The frequency dependence of the kinetic energy W of the ion relates to its orbital radius R in the following way:

$$\mathrm{W} = \frac{1}{2}\mathrm{mv}^2 = \frac{1}{2}\mathrm{m}(2\pi \mathrm{R f_{rev}})^2 = \frac{1}{2}\mathrm{m}(2\pi \mathrm{R}\frac{\mathrm{f_{rf}}}{\mathrm{h}})^2 \tag{3.25}$$

thus, given cyclotron size (R), $\mathrm{f_{rf}}$ and h set the limit for the acceleration range.

The revolution frequency decreases with energy and the condition of synchronism with the oscillating voltage, $\mathrm{f_{rf}} = \mathrm{h f_{rev}}$, is only fulfilled at one particular radius in the course of acceleration, where $\omega_{\mathrm{rf}} = qB/m$ (Fig. 3.14). Upstream and downstream of that radius, out-phasing $\Delta\phi$ builds-up turn after turn, decreasing in a first stage

(towards lower voltages in Fig. 3.14-right) and then increasing back to $\phi = \pi/2$ and beyond towards π. Beyond $\phi = \pi$ the RF voltage is decelerating.

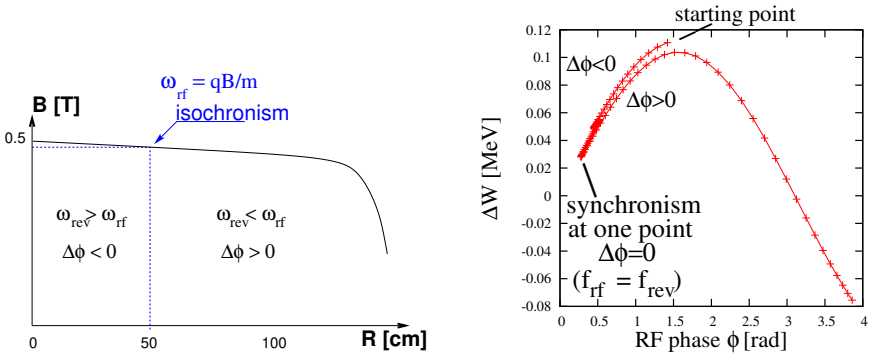

Fig. 3.14 A sketch of the synchronism condition at one point (left, h=1 assumed), and the span in phase of the energy gain $\Delta W = q\hat{V}\sin\phi$ over the acceleration cycle (right). ϕ is the phase of the RF sine wave at arrival of the particle at the accelerating gap (the vertical separation of the two $\Delta W(\phi)$ branches on the right ($\Delta\phi < 0$ and $\Delta\phi > 0$) is artificial, this is for clarity, they are actually superimposed)

Differentiating the particle phase at the RF gap (Eq. 3.24), over a half-turn, with $\omega_{\rm rev}$ constant between two gap passages, one gets $\dot{\phi} = \omega_{\rm rf} - \omega_{rev}$. Between two gap passages on the other hand, $\Delta\phi = \dot{\phi}\Delta T = \dot{\phi}T_{\rm rev}/2 = \dot{\phi}\frac{\pi R}{v}$, yielding a phase-shift of

$$\text{half-turn} \quad \Delta\phi = \pi\left(\frac{\omega_{\rm rf}}{\omega_{\rm rev}(\rm R)} - 1\right) = \pi\left(\frac{\rm m\omega_{rf}}{\rm qB(R)} - 1\right) \tag{3.26}$$

The out-phasing is thus a gap-after-gap, cumulative effect. Due to this the classical cyclotron requires quick acceleration (limited number of turns), which means high voltage (tens to hundreds of kVolts). As expected, with $\omega_{\rm rf}$ and B constant, ϕ presents a minimum ($\dot{\phi} = 0$) at $\omega_{\rm rf} = \omega_{\rm rev} = \frac{\rm qB}{\rm m}$ where exact isochronism is reached (Fig. 3.14). The upper limit to ϕ is set by the condition $\Delta W > 0$: acceleration.

The cyclotron equation determines the achievable energy range, depending on the injection energy E_0, the RF phase at injection ϕ_0, the RF frequency $\omega_{\rm rf}$ and gap voltage $\hat{V}$, following [12]

$$\cos\phi = \cos\phi_0 + \pi\left[1 - \frac{\omega_{\rm rf}}{\omega_{rev}}\frac{E + E_0}{2M}\right]\frac{E - E_0}{q\hat{V}} \tag{3.27}$$

(E=E_k + M is the total energy, M is the rest mass, the index 0 denotes injection parameters) and is represented in Fig. 3.15 for various values of the RF voltage and phase at injection ϕ_0.

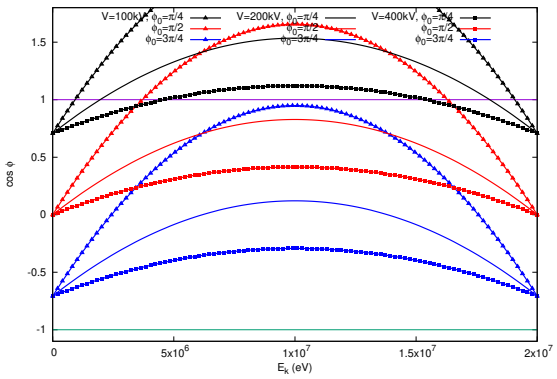

Fig. 3.15 A graph of the cyclotron equation (Eq. 3.27), for a few different RF settings. The sole settings resulting in a $\cos\phi$ curve comprised in $[-1, 1]$ allow complete acceleration from injection to top energy. For instance, for injection $\phi_0 = \pi/4$, acceleration to 20 MeV is not possible (upper three curves). Acceleration to 20 MeV works with $\phi_0 = 3\pi/4$, with as low as 100 kV/gap (lower three curves)

3.1.4 Extraction

From $R = p/qB$ and assuming constant field (legitimate in the presence of a very small field index), with kinetic energy $E_k = p^2/2M$ in the non-relativistic approximation ($E_k \ll M$), one gets

$$\frac{dR}{R} = \frac{1}{2}\frac{dE_k}{E_k} \tag{3.28}$$

Integrating the right hand side equality yields

$$R^2 = R_0^2 \frac{E_k}{E_{k,0}} \tag{3.29}$$

with R_0, $E_{k,0}$ initial conditions. From Eqs. 3.28, 3.29, assuming $E_{k,0} \ll E_k$ and constant acceleration rate dE_k such that $E_k = n\,dE_k$ after n turns, one gets the scaling laws

$$R \propto \sqrt{n}, \qquad dR \propto \frac{R}{E_k} \propto \frac{1}{R} \propto dE_k, \qquad \frac{dR}{dn} = \frac{R}{2n} \tag{3.30}$$

so that, in particular, the turn separation dR/dn is proportional to the average orbit radius R and to the energy gain per turn.

The radial distance between successive turns decreases with energy, toward zero (Fig. 3.16), eventually resulting in insufficient spacing for insertion of an extraction septum.

Betatron modulation

Consider a particle bunch injected in the cyclotron with some (x_0, x_0') conditions, and assume very slow acceleration. While accelerated the bunch undergoes a betatron motion around the local closed orbit, following Eq. 3.15. Observed at some azimuth

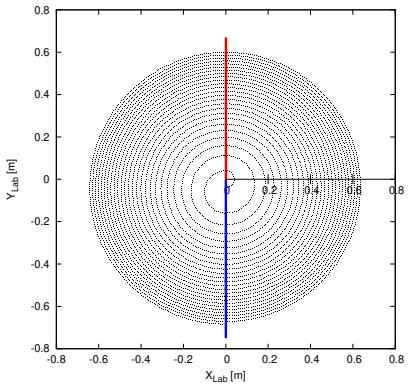

Fig. 3.16 The radial distance between successive turns decreases with energy, in inverse proportion to the orbit radius

s, this betatron oscillation modulates the distance of the bunch to the local reference closed orbit, moving it outward or inward depending on the turn number, which means a modulation of the distance between the accelerated turns: an effect that can be exploited for increasing the separation of consecutive orbits at extraction to enhance the extraction efficiency [8].

3.1.5 Spin Dance

An effect of a magnetic field $\mathbf{B}$ on a spin angular momentum $\mathbf{S}$, as a consequence of the resulting torque, is the spin precession, around the precession vector (Sec. 20.6.1)

$$\boldsymbol{\omega}_{\rm sp} = \frac{q}{m}\,\left[\mathbf{B} + G(\mathbf{B}_{\parallel} + \gamma\mathbf{B}_{\perp})\right] \tag{3.31}$$

at an angular frequency $|\boldsymbol{\omega}_{\rm sp}|$, with $\mathbf{B} = \mathbf{B}_{\parallel} + \mathbf{B}_{\perp}$, $\mathbf{B}_{\parallel}$ and $\mathbf{B}_{\perp}$ the magnetic field components respectively parallel and normal to the particle velocity, and G the anomalous gyromagnetic factor:

G=1.7928474 (proton), -0.178 (Li), -0.143 (deuteron), -4.184 (^{3}He) ...

The spin precession in $\mathbf{B}$ satisfies the Thomas-BMT differential equation

$$\frac{d\mathbf{S}}{dt} = \mathbf{S} \times \boldsymbol{\omega}_{\rm sp} \tag{3.32}$$

If the particle moves in the median plane of a cyclotron then $\mathbf{B}_{\parallel} = 0$ and the precession axis is parallel to the magnetic field vector, $\mathbf{B}_y$, namely $\boldsymbol{\omega}_{\rm sp} = \frac{q}{m}(1 + G\gamma)\mathbf{B}_y$. The precession angle writes

$$\theta_{\rm sp,\,Lab} = \frac{1}{v}\int \omega_{\rm sp}\, ds = (1 + G\gamma)\frac{\int B\, ds}{BR} = (1 + G\gamma)\alpha \tag{3.33}$$

with α the trajectory bend angle (Fig. 3.17). The precession angle in the moving

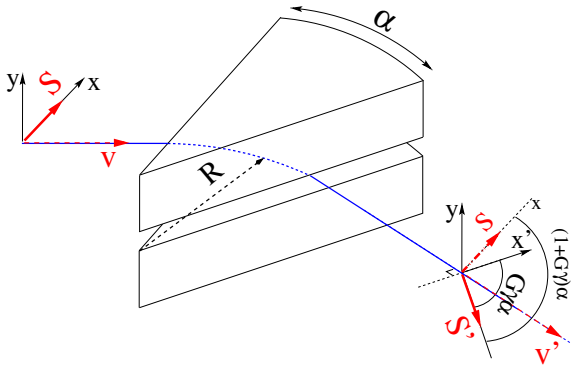

Fig. 3.17 Spin and velocity vector precession in a constant field, from **S** to **S′** and **v** to **v′** respectively. In the moving frame the spin precession along the arc $\mathcal{L} = R\alpha$ is $G\gamma\alpha$, in the laboratory frame the spin precesses by $(1 + G\gamma)\alpha$

frame (the latter rotates by an angle α across the magnet) is

$$\theta_{\mathrm{sp}} = G\gamma\alpha \tag{3.34}$$

from what it results that the number of precessions per turn is $G\gamma$. By analogy with the betatron tune (the number of sinusoidal oscillations per turn around the reference circle, Eq. 3.17) this defines the spin tune

$$\nu_{\mathrm{sp}} = G\gamma \tag{3.35}$$

3.2 Exercises

Preliminaries

- Zgoubi users' guide at hand, when setting up the input data files to work out the exercises, is a must-have. PART B of the guide in particular, details the formatting of the input data lists following keywords (a few keywords only, for instance FAISCEAU, MARKER, YMY, do not require additional data), and gives the units to be used.
- Regarding keywords: by "keyword" it is meant, the name of the optical elements, or I/O procedures, or commands, as they appear in a simulation input data file. Keywords are most of the time referred to without any additional explanation: it is understood that the users' guide is at hand, and details regarding the use and functioning to be sought there: in PART A of the guide, as to what a particular keyword does and how it does it; in PART B as to the formatting of the data list under a particular keyword. The users' guide INDEX is a convenient tool to navigate amongst keywords. A complete list may also be found in the "Glossary of Keywords", at the begining of both PART A and PART B of the users' guide, and an overview of what they can be used at is given in "Optical elements versus keywords".
  - The concise notation KEYWORDS[ARGUMENT1, ARGUMENT2, ...] used in the exercise: it follows the nomenclature of the Users' Guide, Part B. Consider a couple of examples:
    - OBJET[KOBJ=1] stands for keyword OBJET, and the value of KOBJ=1 retained here;
    - OPTIONS[CONSTY=ON] stands for keyword OPTIONS, and the option retained here, CONSTY, switched ON.
  - The keyword INCLUDE is used in many simulation input data files. The reason is mostly to reduce the length of these files (which would otherwise be prohibitively voluminous). Just as with the Latex, or Fortran, "include" command, a segment of an optical sequence subject to an INCLUDE may always be replaced by that very sequence segment.
- Coordinate Systems: two sets of coordinate notations are used in the exercises,
  - on the one hand (and, in the Solutions Section mostly), zgoubi's (Y,T,Z,P,X,D) coordinates in the optical element reference frame (O;X,Y,Z), the very frame in which the optical element field $\mathbf{E}(X, Y, Z)$ and/or $\mathbf{B}(X, Y, Z)$ is defined (the origin for X depends on the optical element). Particle coordinates in this frame can be
    - either Cartesian, in which case X, Y (angle T) and Z (angle P) denote respectively the longitudinal, transverse horizontal and vertical coordinates,
    - or cylindrical, in which case, given m the projection of particle position M in the Z=0 plane, Y denotes the radius: $Y = |\mathbf{Om}|$, whereas X denotes the

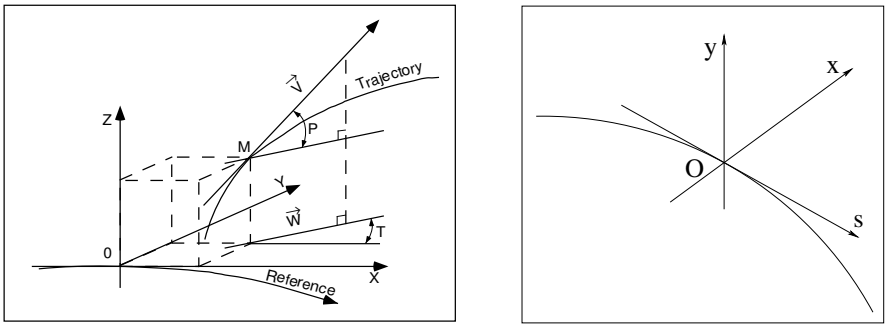

Fig. 3.18 Zgoubi Cartesian frame (O;X,Y,Z), and moving frame (O;s,x,y)

OX-**Om** angle (and, yes, the nature of the variables named X and Y in the source code does change);

Note: the sixth zgoubi's coordinate above is

$$D = \frac{\text{particle rigidity}}{BORO}$$

with BORO a reference rigidity, the very first numerical datum to appear in any zgoubi sequence, as part of the definition of initial particle coordinates by OBJET or MCOBJET. BORO may sometimes be denoted $B\rho_{\text{ref}}$, depending upon the context. Note that D-1 identifies with the above $\delta p/p$.

– on the other hand (and, in the exercise assignments mostly), the conventional (x,x',y,y',δl,$\delta p/p$) coordinates in the moving frame (O;s,x,y) or close variants.

Comments are introduced wherever deemed necessary (hopefully, often enough) in an effort to lift potential ambiguities regarding coordinate notations.

3.1 Modeling a Cyclotron Dipole: Field Map

In this exercise, a cyclotron dipole field is simulated using a field map. A field map is an easy way to simulate a magnet, this is a major interest of the method. It can account for fancy geometries and fields, including field index and non-linearities, field defects. Depending on field symmetries it may be 1-, 2-, or 3-dimensional. It can be generated using mathematical field models, or from magnet computation codes, or from magnetic measurements. In this exercise a model of a cyclotron field is devised using such field map method. The model is based on a calculated two-dimensional map of the mid-plane field, with 180 deg or 60 deg angular extent; TOSCA keyword is used to raytrace through these maps.

The first step in this exercise consists in fabricating that field map.

A 2-dimensional m(R, θ) polar meshing of the median plane is considered (Fig. 3.19). It is defined in a (O; X, Y) frame and covers a 180^0 sector (or 60 deg, in some of the exercises). The median plane field map provides the values of the field components B_Z(R, θ) normal to the $Z = 0$ plane, at the nodes of the mesh. Note

that a single 360^o field map could be used instead, however implementing two 180^o sectors will allow further insertion of an accelerating gap, between the two 180^0 sectors. Computation of the field along (R, θ) particle trajectories in the (O;X,Y,Z) frame is performed from the field map data, using interpolation techniques [13].

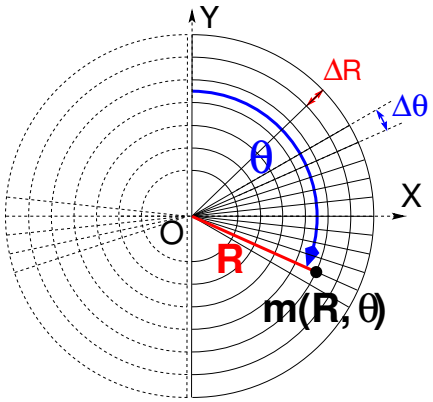

Fig. 3.19 Principle of a field map in a polar coordinate system, covering a 180^o sector (over the right hand side dee). The mesh nodes m(R, θ) are distant ΔR radially, $\Delta\theta$ azimuthally. The map is used twice, so covering the 360^o cyclotron dipole as sketched here, while allowing further insertion of an accelerating gap between the two dees

(a) Construct a 180^o two-dimensional map of a median plane field $B_Z(R, \theta)$, proper to simulate the field in a cyclotron as sketched in Fig. 3.1. Use a uniform mesh in a polar coordinate system (R, θ) as sketched in Fig. 3.19, covering from R=1 to 76 cm. Take a radial increment of the mesh $\Delta R = 0.5$ cm, azimuthal increment $\Delta\theta = 0.5$ cm/RM, RM some arbitrary reference radius (say, 50 cm, here), and constant axial field $B_Z = 0.5$ T. The appropriate 6-column formatting of the field map data for TOSCA to read them is the following:

$$R\cos\theta,\ Z,\ R\sin\theta,\ BY,\ BZ,\ BX$$

with θ varying first, R varying second in that list. Z is the vertical direction (normal to the map mesh), $Z \equiv 0$.

Produce a graph of $B_Z(R, \theta)$.

(b) Raytrace a few concentric circular mid-plane trajectories centered on the center of the dipole, ranging in $10 \le R \le 80$ cm. Produce a graph of these concentric trajectories in the $(O; X, Y)$ laboratory frame. Initial coordinates can be defined using OBJET, particle coordinates along trajectories during the stepwise raytracing can be logged in zgoubi.plt by setting IL=2 under TOSCA.

Explain why it is possible to push the raytracing beyond the 76 cm radius field map extent, without loss of accuracy.

(c) Compute the orbit radius R and the revolution period T_{rev} as a function of kinetic energy E_k, or rigidity BR. Produce a graph, including for comparison the theoretical dependence of T_{rev}. Explain what causes the slow increase of revolution period with energy.

(d) Check the effect of the density of the mesh (the choice of ΔR and $\Delta\theta$ values, *i.e.*, the number of nodes $N_\theta \times N_R = (1 + \frac{180^o}{\Delta\theta}) \times (1 + \frac{80\,\text{cm}}{\Delta R})$), on the accuracy of the trajectory and time-of-flight computation.

(e) Consider a mesh with such ΔR, $\Delta\theta$ density as to ensure reasonably good convergence of the numerical resolution of the differential equation of motion [13, Eq. 1.2.4].

Check the effect of the integration step size on the accuracy of the trajectory and time-of-flight computation, by considering a small $\Delta s = 1\,\text{cm}$ and a large $\Delta s = 20\,\text{cm}$, at 200 keV and 5 MeV (assume proton).

(f) Consider a periodic orbit, thus its radius R should remain unchanged after stepwise integration of the motion over a turn. However, the size Δs of the numerical integration step has an effect on the final value of the radius:

for two different cases, 200 keV (a small orbit) and 5 MeV (a larger one), provide the dependence of the relative error $\delta R/R$ after one turn, on the integration step size Δs (consider a series of Δs values in a range $\Delta s : \ 0.1\,\text{mm} \rightarrow 20\,\text{cm}$). Plot the two $\frac{\delta R}{R}(\Delta s)$ curves (200 keV and 5 MeV), explain their upward concavity.

3.2 Modeling a Cyclotron Dipole: Analytical

This exercise is similar to exercise 3.1, the difference is that an analytical modeling of the field is used here, rather than a field map. The same polar coordinate system (R, θ, Z) is considered, with vertical axis Z normal to the (R, θ) plane (Fig. 3.20).

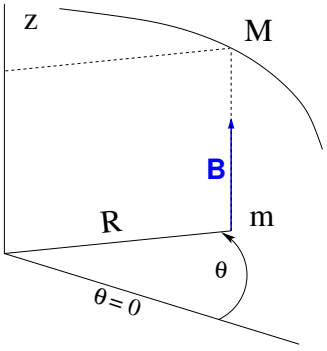

Fig. 3.20 Polar frame. DIPOLE provides the value $B_Z(m)$ of the median plane field at m, projection of particle position $M(R, \theta, Z)$ in the median plane (R, θ)

The vector field $\mathbf{B}(\text{R}, \theta, \text{Z})$ at any location $M(R, \theta, Z)$ of a particle along its trajectory is modeled using DIPOLE (a convenient choice among other possibilities found in zgoubi optical element library). DIPOLE provides the Z-parallel median plane field $\mathbf{B}(\text{R}, \theta, \text{Z} = 0) \equiv \mathbf{B}_\text{Z}(\text{R}, \theta, \text{Z} = 0)$, and $\mathbf{B}(\text{R}, \theta, \text{Z})$ off the median plane is obtained by Taylor expansion (accounting for Maxwell's equations).

(a) Simulate a 180^o sector dipole; DIPOLE requires a reference radius, RM, for the sake of consistency with other exercises, it is suggested to take RM=50 cm. Take a constant axial field $\text{B}_\text{Z} = 0.5\,\text{T}$.

Explain the various data (geometry, role of RM, field and field indices, fringe fields, integration step size, etc.) that define the field simulation in DIPOLE - refer to the Users' Guide [13].

Produce a graph of $\text{B}_\text{Z}(\text{R}, \theta)$.

(b) Repeat question (b) of exercise 3.1.

(c) Repeat question (c) of exercise 3.1.

(d) As in question (e) of exercise 3.1, check the effect of the integration step size on the accuracy of the trajectory and time-of-flight computation.

Repeat question (f) of exercise 3.1.

(e) From the two series of results (exercise 3.1 and the present one), comment on various pros and cons of the two methods, field map versus analytical field model.

3.3 Geometrical Focusing

Because the field is constant over the all space ($\mathbf{B} \equiv \mathbf{B}_Z$ and $|\mathbf{B}_Z|$ =constant, $\forall$ X, Y, Z), there is no vertical focusing: any trajectory with a non-zero vertical angle would spiral away, vertically, with constant pitch angle.

(a) Using the foregoing field model, verify that this is what the numerical integration yields.

Produce a 3-D graph of the trajectory, superpose theory (use the parametric equations of motion) and numerical integration.

(b) Instead, horizontal motion features geometrical focusing, this is due to the trajectory curvature. Show the geometrical focusing graphically.

3.4 Relativistic Kinematic Relationships

In the subsequent exercises, relativistic kinematic quantities will be used, this exercises introduces some differential relations between them which will also be resorted to.

(a) Demonstrate the following relativistic relations (M=rest mass, E_k=kinetic energy, $E = E_k + M$, c=1; γ may vary in electrostatic elements or in the RF cavities of an accelerator):

$$\frac{\mathrm{dp}}{\mathrm{p}} = \frac{1}{\beta^2}\frac{\mathrm{dE}}{\mathrm{E}}, \quad \mathrm{dp} = \frac{\mathrm{dE}}{\beta}$$

$$\frac{\mathrm{dv}}{\mathrm{v}} = \frac{\mathrm{d}\beta}{\beta} = \frac{1}{\gamma^2}\frac{\mathrm{dp}}{\mathrm{p}} = \frac{1}{\beta^2\gamma^2}\frac{\mathrm{dE}}{\mathrm{E}} = \frac{1}{\beta^2\gamma^2}\frac{\mathrm{d}\gamma}{\gamma}$$

$$\frac{\mathrm{d}\gamma}{\gamma} = \frac{\mathrm{dE}}{\mathrm{E}} = \frac{\mathrm{dM}\gamma}{\mathrm{M}\gamma} = \frac{\mathrm{dE_k}}{\mathrm{E_k} + \mathrm{M}}$$

$$\frac{\mathrm{dE}}{\mathrm{E} - \mathrm{M}} = \frac{\mathrm{dE_k}}{\mathrm{E_k}} = \frac{\gamma + 1}{\gamma}\frac{\mathrm{dp}}{\mathrm{p}}$$

(b) Produce the evolution of these quantities numerically, compare these numerical results with theoretical expectations from (a).

(c) Using the random particle generator MCOBJET, produce a 2×10^4 bunch of protons with Gaussian dp/p, $\sigma_{\mathrm{dp/p}} = 10^{-3}$. Plot some of the densities above and check the equalities in (a).

3.5 Resonant Acceleration

Based on the earlier dipole sector, using indifferently a field map or an analytical model of the field, introduce an accelerating gap between the two dees with peak voltage 100 kV. Assume that particle motion does not depend on RF phase: the boost through the gap is the same at all passes, CAVITE[IOPT=3] can be used for that.

(a) Accelerate a proton with initial kinetic energy 20 keV, up to 5 MeV, take harmonic h=1. Produce a graph of the accelerated trajectory in a (O; X, Y) frame similar to that in Fig. 3.19.

(b) Plot the proton momentum p and total energy E as a function of its kinetic energy, both from this numerical experiment (raytracing data can be stored using FAISTORE) and from theory, everything on the same graph.

(c) Plot the normalized velocity $\beta = \mathrm{v}/\mathrm{c}$ as a function of kinetic energy, both numerical and theoretical, and in the latter case both classical and relativistic.

(d) Plot the relative change in velocity $\Delta\beta/\beta$ and the relative change in circumference $\Delta C/C$, as a function of kinetic energy. both numerical and theoretical. From their evolution, conclude that the time of flight increases with energy.

3.6 Resonant Acceleration (2)

Re-do the previous exercise, assuming a harmonic h=3 RF frequency.

3.7 Visit High Energies

Forget the fact that this not possible in a classical cyclotron (use CAVITE[IOPT=3]), and push proton energy to 3 GeV kinetic, re-do questions (a) to (d) of Ex. 3.5.

Note:

- pushing the energy in this manner is only possible if acceleration at the gap is independent of particle phase, hence the necessary choice of CAVITE[IOPT=3],
- if a field map model is used, it is perhaps, or perhaps not, necessary to extend the radial extent of the mesh to encompass the spiraling trajectory up to 3 GeV - please clarify that point,
- in the case the analytical model DIPOLE is used instead, surely no modification is needed, its data remain unchanged, figure that out.

3.8 Spin Dance

(a) From the analogy between the vector precession equations,

$$\dot{\mathbf{v}} = \frac{q}{m}\mathbf{v}\times\mathbf{B}, \qquad \text{particle velocity vector, on the one hand}$$

$$\dot{\mathbf{S}} = \mathbf{S}\times\boldsymbol{\omega}_{\mathrm{sp}}, \qquad \text{particle spin vector, on the other hand (Eq. 20.28),}$$

and from the expression for the particle trajectory rotation angle $\alpha = \int B\,ds/BR$ as stems from the former, deduce the expression for the spin rotation angle in constant vertical B field - no calculations needed.

In the following the cyclotron model of exercise 3.1 or 3.2 indifferently can be used.

(b) Add spin transport, using SPNTRK. Produce a listing (zgoubi.res) of a simulation, including spin outcomes.

Note: PARTICUL is necessary here, in order for the equation of motion to be solved [13, Sec. 2]. SPNPRT can be used to have local spin coordinates listed in zgoubi.res (at the manner FAISCEAU lists particle coordinates).

(c) Consider proton case, initial spin longitudinal, compute the spin precession over one revolution, as a function of energy over a range 12 keV→5 MeV. Give a graphical comparison with theory.

FAISTORE can be used to store local particle data, which include spin coordinates, in a zgoubi.fai style output file. IL=2 can be used to obtain a print out of particle motion data to zgoubi.plt during stepwise integration.

(d) Inject a proton with longitudinal initial spin $\mathbf{S}_i$. Give a graphic of the longitudinal spin component motion as a function of azimuthal angle, over a few turns around the ring. Deduce the spin tune from this computation. Repeat for a couple of different energies.

Place both FAISCEAU and SPNPRT commands right after the first dipole sector, and use them to check the spin rotation and its relationship to particle rotation, right after the first passage through that first sector.

(e) Spin dance: the optical sequence here is assumed to be a complete turn (*i.e.*, six DIPOLEs if a 60 deg DIPOLE model is used). Inject an initial spin at an angle from the horizontal plane (this is in order to have a non-zero vertical component), produce a 3-D animation of the spin dance around the ring, over a few turns.

(f) Repeat questions (b-e) for two additional particles: deuteron (much slower spin precession), $^3He^{2+}$ (much faster spin precession).

3.9 Synchronized Spin Torque

A synchronized spin kick is superimposed on orbital motion. A input data file file accounting the simulation of a complete cyclotron is considered as in (e), for instance six 60 degree DIPOLEs, or two 180 degree DIPOLEs, etc.

Insert a spin rotation of a few degrees around the longitudinal axis, at the end of the optical sequence (*i.e.*, after one orbit around the cyclotron). SPINR can be used for that, to avoid any orbital effect. Track 4 particles on their closed orbit, with respective energies 0.2, 108.412, 118.878 and 160.746 MeV.

Produce a graph of the motion of the vertical spin component S_y along the circular orbit.

Produce a graph of the spin vector motion on a sphere.

Explain the results.

3.10 Introducing a Radial Field Index

(a) Reproduce Fig. 3.11.

(b) Ray trace over a few turns with some $-1 < k < 0$ value, to show the sinusoidal horizontal motion. Show the horizontal motion instability when $k < -1$.

(c) Add vertical motion and show the vertical sinusoidal oscillation with $k < 0$, show the vertical instability if $k > 0$.

3.11 Weak Focusing

(a) Consider a 60^o sector as in earlier exercises (building a field map as in exercise 3.1, or using DIPOLE as in exercise 3.2), construct the sector accounting for a non-zero radial index k in order to introduce vertical focusing, say $k = -0.03$, assume a reference radius R_0 for a reference energy of 200 keV (R_0 and B_0 are required in order to define the index k, Eq. 3.12). Raytrace that 200 keV reference orbit, plot it in the lab frame: make sure it comes out as expected, namely, constant radius, final and initial angles equal (normally null given the working hypotheses, as established in previous exercises).

(b) Find and plot the radius dependence of orbit rigidity, BR(R), from raytracing over a BR range covering 20 keV to 5 MeV.

(c) Produce a graph of the paraxial axial motion of a 1 MeV proton, over a few turns (use IL=2 under TOSCA to have stepwise integration data logged in zgoubi.plt). Check the effect of the focusing strength by comparing the trajectories for a few different index values, including close to -1 and close to 0.

(d) Produce a graph of the magnetic field experienced by the particle along these trajectories.

3.12 Loss of Isochronism

Compare on a common graphic the revolution period $T_{rev}(R)$ for a field index value $k \approx -0.95,\ -0.5,\ -0.03,\ 0^-$. The scan method of exercise 3.11, based on REBELOTE, can be referred to.

3.13 Particle Trajectories

In this exercise individual particle trajectories are computed. DIPOLE or TOSCA can be used, indifferently. No acceleration in this exercise, particles cycle around the cyclotron at constant energy.

(a) Produce a graph of the horizontal and vertical trajectory components x(s) and y(s) of a particle with rigidity close to $BR(R_0)$ (R_o is the reference radius in the definition of the index k), over a few turns around the cyclotron. From the number of turns, give an estimate of the wave numbers. Check the agreement with the expected $\nu_R(k)$, $\nu_y(k)$ values from Eq. 3.17.

Consider particle energies of 1 MeV and 5 MeV, far from the reference kinetic energy $E(R_0)$; the wave numbers change with energy: could that be expected? Find their theoretical values, compare with numerical outcomes.

(b) In the former case, 200 keV energy, plot as a function of s the difference between x(s) from raytracing and its values from Eq. 3.15. Same for y(s) compared to Eq. 3.16. Is there agreement? (use the option IL=2 to store particle coordinates in zgoubi.plt, step-by-step).

3.14 Energy Dependence of Wave Numbers

Perform a scan of the wave numbers over 200 keV−5 MeV energy interval, computed using MATRIX, and using REBELOTE to repeat MATRIX computation for a series of energy values.

3.15 Phase Space Motion, Fourier Analysis

This exercise introduces to phase space and phase space motion, and to spectral analysis of particle motion.

Raytrace a particle with small amplitude radial and axial oscillations with respect to the reference circular closed orbit (paraxial motion), at constant energy.

(a) At some fixed azimuth s around the cyclotron, observe the radial excursion (x(n),x'(n)) of the particle as it cycles around for many turns (n is the turn number) (use FAISTORE to store particle coordinates in zgoubi.fai, turn by turn). Produce a graph of $(x(n), x'(n))$ in the transverse phase-space (x, x').

Repeat for (y,y').

(b) From the trajectory equation (Eq. 3.15, radial motion, or Eq. 3.16, axial motion), show that particle motion in phase space is on an ellipse. Calculate the ellipse parameters. Verify graphically that it superposes on the particle motion from multiturn raytracing.

(c) Compute the radial and axial wave numbers by Fourier analysis of respectively the x(n) and the y(n) motion. Check the agreement with the expected $\nu_{\mathrm{R}}(\mathrm{k})$, $\nu_{\mathrm{y}}(\mathrm{k})$ values from theory.

(d) Constant energy motion spectrum:

(i) there is an indetermination on the value of the wave number, from the Fourier analysis, explain

(ii) give a theoretical calculation of the accuracy on the position of the peak from the DFT technique. Check this against the numerical computation by varying the spectrum sampling in the DFT series

(iii) explain the origin of the $\sin \mathrm{u}/\mathrm{u}$ shape of the spectrum. Calculate the spacing between the zeroes, from theory, compare with the zeroes of the numerical DFT.

3.16 RF Phase at the Accelerating Gap

(a) Consider the cyclotron model of exercise 3.11: two dees, double accelerating gap, field index k = −0.03 defined at $R_0 = 50\,\mathrm{cm}$, field $\mathrm{B}_0 = 5\,\mathrm{kG}$ on that radius.

Raytrace a proton trajectory from 1 to 5 MeV: get the turn-by-turn phase-shift at the gaps, compare with (Eq. 3.26)

$$\text{half-turn} \quad \Delta\phi = \pi \left(\frac{\omega_{\mathrm{rf}}}{\omega_{\mathrm{rev}}(R)} - 1 \right) = \pi \left(\frac{m\omega_{\mathrm{rf}}}{qB(R)} - 1 \right)$$

Produce a similar diagram $\Delta\mathrm{W}(\phi)$ to Fig. 3.14-right.

Accelerate over more turns, observe the particle decelerate.

(b) Repeat (a) for the index definition of exercise 3.11: k=-0.03, defined on the 200 keV injection radius $R_0 = 12.924888\,\mathrm{cm}$, with $B_0 = 5\,\mathrm{kG}$.

3.17 The Cyclotron Equation

Cyclotron model settings of exercise 3.5 are first considered in questions (a) to (c): two dees, double accelerating gap, uniform field $B = 0.5\,\mathrm{T}$ (a field map or analytical field modeling can be used, indifferently). In question (d) a field index is introduced.

(a) Set up an input data file for the simulation of a proton acceleration from 0.2 to 20 MeV. In particular, assume that $\cos(\phi)$ reaches its maximum value at $\mathrm{W}_{\mathrm{m}} = 10\,\mathrm{MeV}$; find the RF voltage frequency from $\mathrm{d}(\cos\phi)/\mathrm{dW} = 0$ at W_{m}.

(b) Give a graph of the energy-phase relationship (Eq. 3.27)

$$\cos\phi = \cos\phi_0 + \pi \left[1 - \frac{\omega_{\mathrm{rf}}}{\omega_{rev}} \frac{E + E_0}{2M} \right] \frac{E - E_0}{q\hat{V}}$$

for $\phi_0 = \frac{3\pi}{4},\ \frac{\pi}{2},\ \frac{\pi}{4}$, from both simulation and theory.

(c) Re-do the exercise using an RF frequency third harmonic of the revolution frequency, in the same double-dee configuration.

(d) Repeat (a) and (b) for the index definition of exercise 3.11: k=-0.03, defined on the 200 keV injection radius $R_0 = 12.924888\,\mathrm{cm}$, with $B_0 = 5\,\mathrm{kG}$.

3.18 Cyclotron Extraction

(a) Acceleration of a proton in a uniform field B=0.5 T is first considered, this is the case of exercise 3.5.

Compute the distance ΔR between turns, as a function of turn number and of energy, over the range $E : 0.02 \rightarrow 5$ MeV. Compare graphically with theoretical expectation.

(b) Assume a beam with Gaussian momentum distribution and *rms* momentum spread $\delta p/p = 10^{-3}$. An extraction septum is placed half-way between two successive turns, plot the percentage of beam loss at extraction, as a function of extraction turn number - COLLIMA can be used for that simulation and for particle counts, it also allows for possible septum thickness.

(c) Repeat (a) and (b) considering a field with index - conditions of exercise 3.10 for instance, $B_0 = 0.5$ T and $k = -0.03$ at $R_0 = R(0.2\,\text{MeV}) = 12.924888$ cm.

(d) Investigate the effect of injection conditions (x_0, x_0') on the modulation of the distance between turns.

Show that, with slow acceleration, the oscillation is minimized for an initial $|x_0'| = |\frac{x_0 \nu_R}{R}|$ [8, p. 133].

3.19 Acceleration and Extraction of a 6-D Polarized Bunch

The cyclotron simulation hypotheses of exercise 3.17-a are considered.

Add a short "high energy" line, say 1 meter, for beam extraction downstream of the cyclotron (which means following REBELOTE in the optical sequence), ending up with a "Beam_Dump" MARKER.

(a) Create a 1,000 particle bunch with the following initial parameters:

- random Gaussian transverse phase space densities, centered on the closed orbit, truncated at 3 sigma, normalized *rms* emittances $\epsilon_Y = \epsilon_Z = 1\,\pi\mu$m, both emittances matched to the 0.2 MeV orbit optics,
- uniform bunch momentum density $0.2\times(1-10^{-3}) \leq p \leq 0.2\times(1+10^{-3})$ MeV, matched to the dispersion, namely (Eq. 3.21), $\Delta x = D\frac{\Delta p}{p}$,
- random uniform longitudinal distribution $-0.5 \leq s \leq 0.5$ mm,

Note: there is two possibilities to create this object, namely, using either (i) MCOBJET, or (ii) OBJET[KOBJ=3] which reads an external file containing particle coordinates.

Add spin tracking request (SPNTRK), all initial spins normal to the bend plane.

Produce a graph of the three initial 2-D phase spaces: (Y,T), (Z,P), (δl,$\delta p/p$, check the matching to the 200 keV optics.

Plot the Y, Z, dp/p, δl and S_Z histograms. Check the distribution parameters.

(b) Accelerate this polarized bunch to 20 MeV, using the following RF conditions:

- 200 kV peak voltage,
- RF harmonic 1,
- initial RF phase $\phi_0 = \pi/4$.

Produce a graph of the three phase spaces as observed downstream of the extraction line. Plot the Y, Z, dp/p, δl and S_Z histograms. Compare the distribution parameters with the initial values.

What causes the spins to spread away from vertical?

References

1. Jones, L., Mills, F., Sessler, A., et al.: Innovation Was Not Enough. World Scientific (2010)
2. Lawrence, E.O., Livingston, M.S., Phys. Rev. 37, 1707 (1931), 1707; Phys. Rev. 38, 136, (1931); Phys. Rev. 40, 19 (1932)
3. Ernest O. Lawrence and M. Stanley Livingston, The Production of High Speed Light Ions Without the Use of High Voltages, Phys. Rev. 40, 19-35 (1932)
4. Livingston, M.S., McMillan, Edwin M.: History of the cyclotron. Physics Today, 12(10) (1959).
   https://escholarship.org/uc/item/29c6p35w
5. Bethe, H. E., Rose, M. E.: Maximum energy obtainable fromcyclotron. Phys. Rev. 52 (1937) 1254
6. Cole, F.T.: O Camelot ! A memoir of the MURA years (April 1, 1994).
   https://accelconf.web.cern.ch/c01/cyc2001/extra/Cole.pdf
7. 4.a L.H.Thomas, *The Paths of Ions in the Cyclotron*, Phys. Rev. 54, 580, (1938)
   4.b M.K. Craddock, *AG focusing in the Thomas cyclotron of* 1938 , Proceedings of PAC09, Vancouver, BC, Canada, FR5REP1
8. Stammbach, T.: Introduction to Cyclotrons. CERN accelerator school, cyclotrons, linacs and their applications. IBM International Education Centre, La Hulpe, Belgium, 28 April-5 May 1994.
9. Baron, E., et al.: The GANIL Injector. Proceedings of the 7th International Conference on Cyclotrons and their Applications, ZÃijrich, Switzerland (1975).
   http://accelconf.web.cern.ch/c75/papers/b-05.pdf
10. Li, C.Y., et al.: A Permanent Magnet System for a Cyclotron used as a mass spectrometer.
11. Lawrence, E.O., Edlefsen, N.E.: On the production of high speed protons. Science, 72, 376-377 (1930)
12. Le Duff, J.: Longitudinal beam dynamics in circular accelerators. CERN Accelerator School, Jyvaskyla, Finland, 7-18 September 1992
13. Méot, F.: Zgoubi Users' Guide.
    https://www.osti.gov/biblio/1062013-zgoubi-users-guide Sourceforge latest version:
    https://sourceforge.net/p/zgoubi/code/HEAD/tree/trunk/guide/Zgoubi.pdf